Appl. Phys. B 65, 459–469 (1997)

Applied Physics B Lasers and Optics

Laser-induced fluorescence study of a xenon Hall thruster

R.J. Cedolin, W.A. Hargus, Jr., P.V. Storm, R.K. Hanson, M.A. Cappelli

Thermosciences Division, Department of Mechanical Engineering, Stanford University, Stanford, CA 94305-3032, USA
(rcedolin@navier.stanford.edu; cap@leland.stanford.edu)

Received: 20 January 1997/Revised version: 12 May 1997

Abstract. Laser-induced fluorescence of the neutral-xenon $6s[3/2]_2^0 \rightarrow 6p[3/2]_2(^3P_2 - ^1D_2)$ transition at 823.2 nm and the xenon-ion $5d[3]_{7/2} \rightarrow 6p[2]_{5/2}^0(^4D_{7/2} - ^4P_{5/2})$ transition is used to measure plasma parameters in the plume of a laboratory-model xenon Hall thruster. The Hall discharge operates nominally at 62 V, 4.2 A, and 3.2 mg s^{-1} xenon flow, with an overall thruster power of 320 W. A tunable semiconductor diode laser and an Ar^+-pumped dye laser are used to probe the respective excited-state transitions. Axial velocity measurements are made at a number of axial and radial locations up to 4.5 cm downstream of the thruster-exit plane and under a variety of thruster operating conditions. Neutral velocities from 100 m s^{-1} to 400 m s^{-1} and ion velocities as high as 12 km s^{-1} are calculated from measured Doppler shifts. The charge-exchange phenomenon evidently does not significantly affect the xenon neutrals. The spectral-line shapes of the ion indicate a spread in ion energies through a non-Maxwellian distribution of axial velocities. Neutral kinetic temperatures of 500 (±200) K are observed under standard operating conditions. Zeeman and Stark effects on the spectral-line shapes, from the thruster's magnetic and electric fields, are not substantial. The measured line center of the ion transition is 16521.23 (±0.02) cm^{-1}.

PACS: 52.70.Kz; 32.70.Jz; 52.75.-d

The use of xenon as a propellant for satellite electric propulsion has stimulated a growing interest in the use of laser diagnostic techniques for xenon plasmas. These techniques are being developed for application to both Kaufman-type ion thrusters and Hall accelerators such as the stationary plasma thruster and the anode layer thruster. Nonintrusive measurements of parameters in the plumes and within the discharge channels of these satellite thrusters are needed to give an insight into the physical processes controlling their operation. Optical diagnostic measurements have been employed successfully in the past to study various plasma properties in electric propulsion devices. The hydrogen arcjet, for example, has been extensively studied using lasers as probes to measure velocity, temperature, and electron number density [1]. Laser-induced fluorescence (LIF) has proven to be a particularly valuable tool in these studies. The high spatial resolution of single-point laser-induced fluorescence is essential in probing nonuniform plasma environments, such as those encountered in electric propulsion devices. Extensive studies of Hall thrusters using this nonintrusive technique should be equally valuable.

We report LIF velocity measurements of singly-ionized and neutral xenon in the plume of a laboratory-model Hall thruster. Spectroscopic diagnostic techniques for xenon are complicated, in general, by the intricate hyperfine structure of xenon spectral transitions. The complicated spectroscopy of xenon does not, however, prevent the use of LIF as a velocity diagnostic. Measurements of xenon-ion velocities from Doppler-shifted LIF spectra have been made previously in a stationary plasma thruster [2]. A tunable AlGaAs semiconductor diode laser and a tunable dye laser are used here to interrogate the plasma downstream of the annulus exit of the Hall thruster operating at 320 to 680 W. Measurements of neutral velocities, ion velocities, as well as other neutral and ion parameters, are important to the validation of physical models [3]. In addition, these measurements are helpful in gaining qualitative information on the performance of the specific thruster being investigated.

We discuss also the effects of plasma properties on the xenon spectral-line shapes, namely the velocity distribution and kinetic temperature, and the magnetic field. Knowledge of the constituent transitions contributing to a spectral-line shape is required to gain insight into the plasma environment through its effect on the spectral distribution of the collected fluorescence. The spectroscopy of two transitions of neutral xenon are well understood. The spectral broadening of the $6s[3/2]_1^0 \rightarrow 6p[1/2]_0(^3P_1 - ^3P_0)$ transition at 828.0 nm has been developed into a number density diagnostic, and the Doppler broadening of the $6s[3/2]_2^0 \rightarrow 6p[3/2]_2(^3P_2 - ^1D_2)$ transition at 823.2 nm has been employed successfully as a kinetic temperature diagnostic in a room-temperature direct-current (dc) glow discharge [4]. Knowledge of the isotopic and nuclear-spin splitting of xenon-ion transitions is more limited. The xenon-ion

$5d[3]_{7/2} \rightarrow 6p[2]^0_{5/2}(^4D_{7/2} - {}^4P_{5/2})$ transition at 605.1 nm is the only transition of the xenon ion for which isotopic and hyperfine structure measurements have been reported [5–7].

1 Theory

The interaction of a laser beam with a plasma may involve the excitation of some atoms to a higher quantum state. Monitoring the fluorescence from these higher states as the laser is tuned over the transition provides a measure of the fluorescence-excitation-line shape, allowing for a nonintrusive reconstruction of a spectral-line shape representative of the plasma conditions. If the species absorbing the laser light has a velocity component along the axis of the laser beam, it absorbs the light at a frequency different from that of stationary absorbers because of the Doppler effect. The magnitude of this frequency shift $\delta\nu_{12}$ depends on the velocity v along the laser beam axis as follows:

$$\delta\nu_{12} = \nu_{12}\frac{v}{c}\,. \tag{1}$$

The Doppler shift of a species' fluorescence profile away from the line center ν_{12} of stationary absorbers is thus a direct measure of the species velocity.

A partial energy level diagram for neutral xenon is shown in Fig. 1. The energy-level values are from [8]. The excited-state, neutral transition probed in this work, arising from the metastable $6s[3/2]^0_2$ level, is indicated. The levels shown on the energy-level diagram are the fine-structure components resulting from electron-spin–orbit interactions. Transitions between these energy levels are hyperfine split into several components from nuclear-spin effects and from isotopic effects. This splitting decomposes the 823.2-nm transition into 21 lines. A model line shape can be constructed by broadening the 21 lines into Voigt profiles and subsequently adding the individual components [4]. The assumption of a Maxwellian velocity distribution of the absorbing atoms within the probe volume allows the modelling of the line shape using a Gaussian component to a Voigt profile. This assumption is reasonable for a dc discharge. However, the assumption of a Maxwellian velocity distribution in the plume of the Hall thruster is not necessarily valid given the highly nonequilibrium nature of this plasma.

As is the case with neutral xenon, the ground state of the xenon ion is not easily accessible to LIF. The excited-state, xenon-ion transition probed is the 605.1-nm transition arising from the metastable $5d[3]_{7/2}(^4D_{7/2})$ state, as shown in Fig. 2. The energy-level values in the figure are from [9]. This transition has 19 isotopic and hyperfine components contributing to its line shape. Nonresonant fluorescence at 529.2 nm is collected from the $6p[2]^0_{5/2}(^4P_{5/2})$ upper state.

The measured LIF signal is given by [10]

$$S_\mathrm{f} = \eta_\mathrm{d}\alpha_\mathrm{c}h\nu_{12}AN_2\,, \tag{2}$$

where η_d is the efficiency of the detection system, α_c takes into account factors involving the collection system, and A is the Einstein coefficient for spontaneous emission of the detected radiation. A two-level rate-equation analysis yields the following result for the upper-level population at steady state [11]:

$$N_2 = \frac{N_1 + N_2}{1 + \frac{g_1}{g_2} + (A+Q)\frac{c}{B_{12}\Phi_\mathrm{H}I_\nu}}\,. \tag{3}$$

Here I_ν is the spectral irradiance (intensity) at frequency ν, and B_{12} is the Einstein stimulated absorption coefficient, $B_{12,\nu} = B_{12}\Phi_\mathrm{H}$ with Φ being the transition's spectral-line

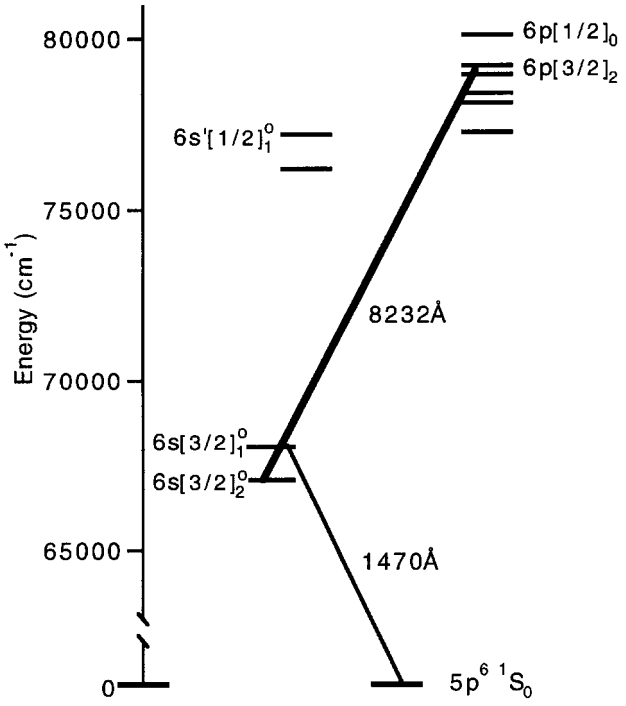

Fig. 1. Partial energy-level diagram of xenon

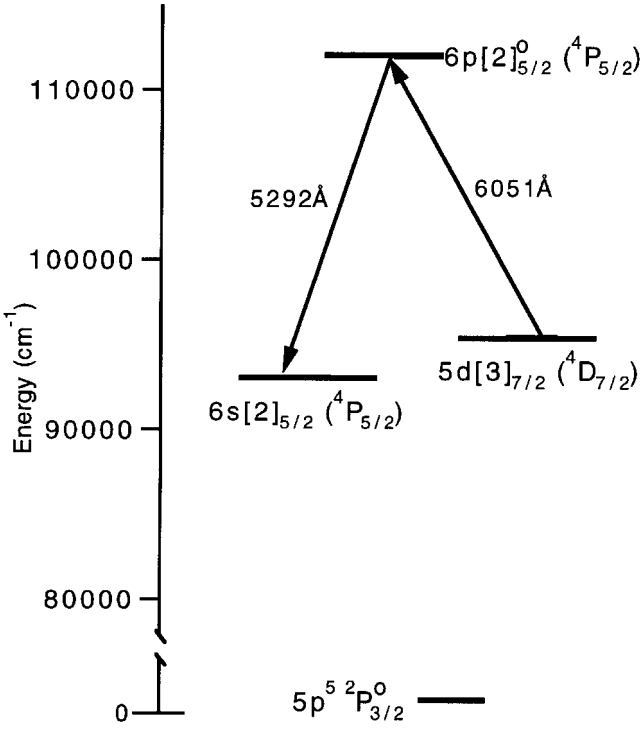

Fig. 2. Partial energy-level diagram of singly-ionized xenon

shape, which accounts for the variation of absorption with laser frequency. The spectral-line shape is determined by the plasma environment of the absorbing atoms. The homogeneous contribution to the line shape Φ_{H}, from collisional interactions between the probed absorbers and other particles and from the inherent uncertainty in assigning an energy to the energy states involved, is the Lorentzian contribution to the Voigt profile. The lower and upper state degeneracies are represented by g_1 and g_2, and Q is the collisional quenching coefficient from the upper state. Assuming a Maxwellian velocity distribution and integrating over all spectral packets [12, 13] to account for a Gaussian, inhomogeneous broadening component results in

$$S_{\mathrm{f}} = \eta_{\mathrm{d}}\alpha_{\mathrm{c}} h\nu_{12}\frac{A}{A+Q}\frac{B_{12}}{c} \times \frac{I_\nu}{\sqrt{(1+I_\nu/I_{\mathrm{sat}})}}(N_1+N_2)\Phi_\nu(a_{\mathrm{S}}, w)\,, \tag{4}$$

with I_{sat} the saturation intensity:

$$I_{\mathrm{sat}} = \frac{\pi c \Delta\nu_{\mathrm{L}}}{2}\frac{A+Q}{B_{12}}\frac{g_2}{g_1+g_2}\,, \tag{5}$$

and $\Phi_\nu(a_{\mathrm{S}}, w)$ the Voigt-line shape with parameter a_{S} [14]. The Voigt w parameter is a nondimensional detuning from line center and the usual Voigt a parameter is defined as

$$a \equiv \sqrt{\ln 2}\frac{\Delta\nu_{\mathrm{L}}}{\Delta\nu_{\mathrm{G}}}\,, \tag{6}$$

with $\Delta\nu_{\mathrm{L}}$ and $\Delta\nu_{\mathrm{G}}$ being the Lorentzian and Gaussian full widths at half maximum (FWHM). The parameter a_{S} is then

$$a_{\mathrm{S}} = a\sqrt{1+\frac{I_\nu}{I_{\mathrm{sat}}}}\,. \tag{7}$$

For low laser intensities, I_{sat} drops out of the above analysis ($I/I_{\mathrm{sat}} \to 0$) and a line shape can be accurately modelled using (4) by summing the Voigt profiles with the a parameter, not a_{S}. A demonstration of the model and fitting procedures for this case can be found in [4]. The different line intensities arise only from different isotopic abundances and different B_{12} values for each nuclear-spin-split component. The relative broadening is only slightly different from the differences in isotopic mass, which affect the Doppler component. The kinetic temperature can, in this case, be extracted easily from the Doppler component supplied by the curve fit of the model.

For higher laser intensities the situation is considerably more complicated. The relative hyperfine-line intensities and their relative broadening in the detected fluorescence are then affected by different I_{sat} values. Saturation or power broadening occurs as there is preferential absorption, and therefore saturation of the signal, when the laser is tuned to one of the line centers. The proximity in energy of the nuclear-spin-split levels would require that a multilevel model be considered in the saturated case; however, Berg and Shackleford [11] find that in an analysis of a four-level model the general behaviour turns out to be the same as for the simpler two-level model. Also, I_{sat} only depends on the collisional quenching from the collection of upper nuclear-spin-split states to the lower collection of states if the collisional transfer rates between the laser-coupled levels and nearby levels are much greater than the quench rate from the upper levels down to the lower levels. The saturated-line shape still contains information on the kinetic temperature and other plasma parameters but this information is not so easily extracted. Other assumptions embodied in (4) are constant laser intensity across the probe volume, negligible radiative trapping – the absorption of the probe volume fluorescence before reaching the detector – and negligible upward collisional excitation.

Local electric and magnetic fields can further affect the spectroscopy of a transition. A magnetic field splits each fine or hyperfine line into a number of lines through Zeeman splitting. An extremely strong electric field can also cause a splitting, as well as a shifting, of spectral lines through Stark effects. Furthermore, perturbations of an atom's energy levels by nearby charged particles lead to a Stark shift as well as Stark broadening of a spectral line.

2 Facility

The Hall-thruster test facility consists of a nonmagnetic, stainless-steel tank approximately 1 m in diameter and 1.5 m in length. Two 50-cm diameter oil-diffusion pumps together provide a nominal pumping speed in air of $35\,000\,\mathrm{l\,s^{-1}}$ and are backed by a $425\text{-}\mathrm{l\,s^{-1}}$ mechanical pump. All pressure measurements are made with an ionization gauge which is not corrected for gas species. The base pressure reading of the system is 10^{-7} torr. While firing the thruster at nominal run conditions with a total of $3.2\,\mathrm{mg\,s^{-1}}$ flow of xenon, the tank pressure reading is 2×10^{-4} torr. These values correspond to a xenon pumping speed of $2000\,\mathrm{l\,s^{-1}}$. The thruster is mounted on a two-axis translation mount within the tank.

The thruster used in this study is a laboratory model based on the design of thrusters being considered for high specific-impulse station-keeping missions. The operating principles of the Hall and related closed-drift thrusters are discussed extensively in the literature [15–20]. Excluding the cathode, the thruster body has an overall width of 95 mm and a height of 120 mm. The thruster body also serves as the magnetic-field circuit. As shown in Fig. 3, there is an inner north magnetic pole and outer south pole surrounding an insulated, annular channel, which is 10 mm wide and 14 mm in depth. Four outer solenoids and one central solenoid generate the magnetic field. The solenoid cores are constructed of mild steel while the front plates (Fig. 3) are made from commercially pure iron. The solenoids consist of cores 6.5 mm in diameter wrapped with 22-gauge, insulated copper magnet wire. The resulting magnetic induction field has a maximum value of 120 G, which occurs at a solenoid current of 2.5 A. The magnetic field strength limitations result from the design of the central core; however, resistive heating in the solenoid coils reduces the maximum continuous current to 2.0 A from the 200-°C temperature limit imposed by the magnet-wire insulation.

The alumina insulator supports the 90-mm diameter, nonmagnetic, stainless-steel anode, which also distributes the propellant into the annulus. Propellant distribution is accomplished by 32 evenly spaced holes each with a diameter of 0.5 mm. The cathode current is produced by an Ion Tech HCN-252 hollow-cathode neutralizer capable of supporting a maximum of 5 A. The neutralizer is mounted on the thruster

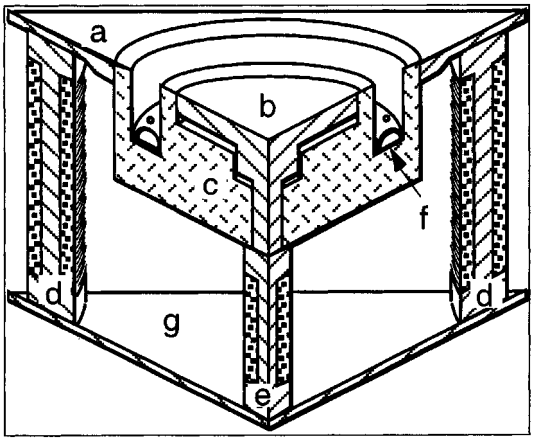

Fig. 3a–g. Laboratory-model Hall thruster: **a** south magnetic pole (front plate); **b** north magnetic pole; **c** alumina plasma insulator; **d** outer solenoids; **e** central solenoid; **f** propellant distribution system and anode; **g** back plate

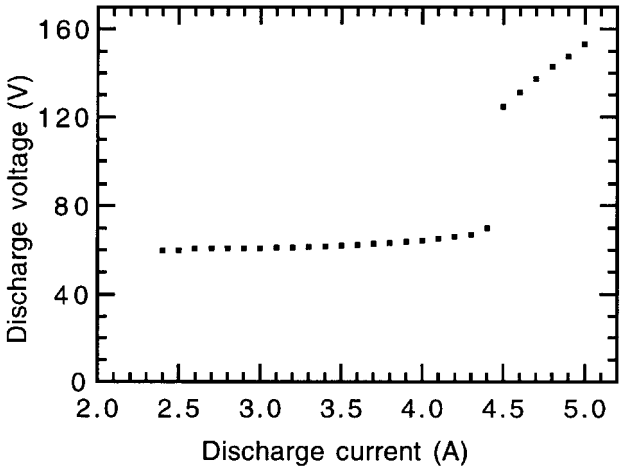

Fig. 4. Current–voltage characteristic for an anode mass-flow rate of $2.9\,\mathrm{mg\,s^{-1}}$ and cathode mass flow of $0.29\,\mathrm{mg\,s^{-1}}$

by a stainless-steel bracket which positions the electron beam to intercept the ion beam at a 30° angle downstream from the vertical approximately 70 mm from the exit of the thruster.

The main discharge is nominally powered by a current-controlled power supply. The cathode requires two power supplies. A variable transformer powers the heating element, supplying 8.5 A at startup and 4.0 A during normal operation. The cathode keeper is supplied with 250 V for startup and approximately 7 V and 250 mA during thruster operation. A current-controlled power supply furnishes power to the solenoids.

Figure 4 shows the current–voltage characteristic of the Hall thruster for nominal operation at $2.9\,\mathrm{mg\,s^{-1}}$ xenon flow through the anode and $0.29\,\mathrm{mg\,s^{-1}}$ through the cathode. The typical voltage knee is evident at a current of approximately 4.3 A [15]. This condition corresponds to approximately 50% of the emitted electrons neutralizing the ion beam, with the remainder supporting the electric field in the channel. The current-equivalent mass flow from the annulus, assuming full ionization, is 2.2 A.

Standard operating conditions for the thruster are as shown in Table 1. Because of limitations in the allowable heat flux to the alumina insulator, power levels are generally limited to below 400 W for the nominal flow rates. This power level allows the thruster to run near the base of the voltage knee of the thruster which according to Kaufman [15] is the optimum operation point for Hall thrusters.

Table 1. Steady state conditions – after 10 run hours

Power to main discharge	260 W	(4.2 A, 62 V)
Power to cathode keeper	1.7 W	(250 mA, 6.9 V)
Power to cathode heater	21 W	(4.15 A, 5 V)
Power to magnetic circuit	38 W	(2.0 A, 19.2 V)
Total power	321 W	
Mass-flow rate to anode	$2.9\,\mathrm{mg\,s^{-1}}$	(30 SCCM)
Mass-flow rate to cathode	$0.29\,\mathrm{mg\,s^{-1}}$	(1.0 SCCM)
Background pressure	2×10^{-4} torr	
Solenoid temperature	206 °C	
Front plate temperature	208 °C	

3 Experiment

3.1 Neutral-xenon measurements

A schematic of the diagnostic setup for the neutral-xenon measurements is shown in Fig. 5. A tunable AlGaAs semiconductor diode laser is the excitation source for the neutral-xenon measurements. Diode lasers are capable of providing typical lasing linewidths of about 10 MHz [21]. The beam first passes through an optical isolator. The laser beam then encounters a beam splitter. The main portion of the beam passing through the beam splitter is redirected into the thruster plume in the axial direction and focused near the thruster exit. The beam is expanded and then brought down to a submillimeter focus by 1000-mm and 750-mm focal-length lenses. About 15 to 20 mW of laser power reaches the probe volume, far exceeding the saturation intensity for the 823-nm transition [4]. This level of laser power is required to provide a reasonable signal level from the neutral xenon in the highly ionized thruster plume. The laser probes the exit of the channel of the thruster on the side opposite the cathode.

The probe volume at the beam focus is imaged onto the entrance slit of a half-meter monochromator by 600-mm and 280-mm focal-length lenses. An iris matches the collection system $f/\#$ to that of the monochromator. The plasma emission and LIF are collected at right angles to the laser beam. The intersection of the collection volume with the laser beam defines the probe volume. A photomultiplier tube detects the LIF along with the background plasma emission. The monochromator is used as a spectral filter, transmitting light over the entire transition while the laser frequency is varied to produce the LIF line shape. The monochromator's slit height determines the extent of the probe volume along the beam axis, which is also the axial plume direction. For one set of neutral-xenon measurements, light was collected over a 10-mm length of the laser beam. For a subsequent set of measurements, this length was reduced to 6 mm. A portion of the laser beam large enough to provide an adequate fluorescence signal needs to be imaged onto the monochromator slit.

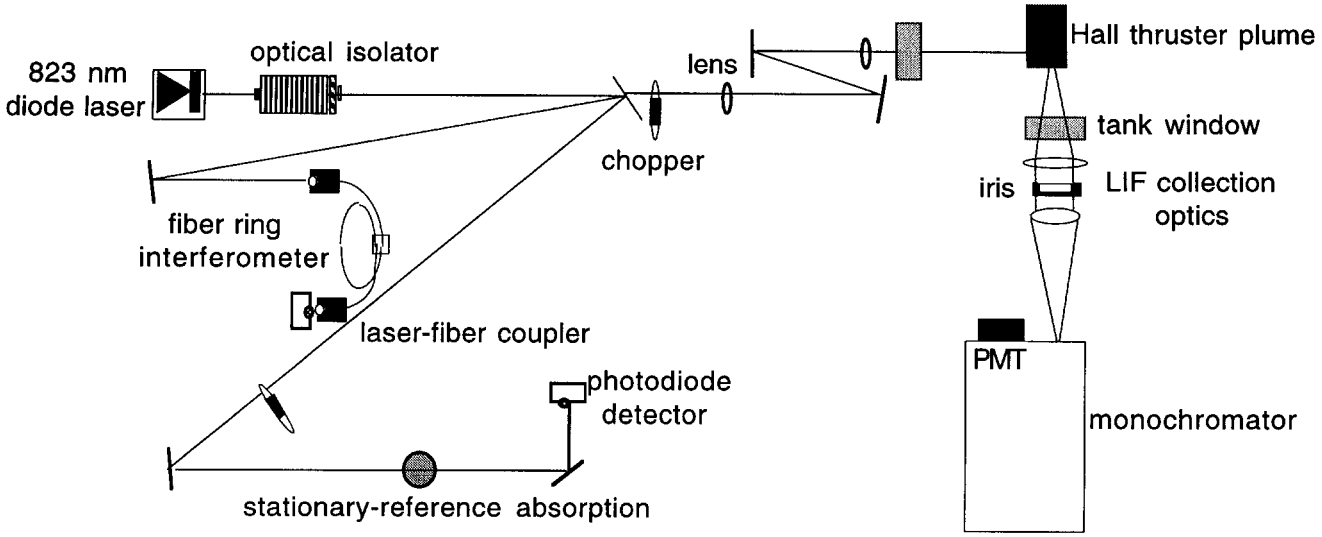

Fig. 5. Schematic of diagnostics setup

A dc discharge in a xenon spectrum tube serves as a stationary xenon-plasma source. One of the two reflections from the beam splitter is redirected through this discharge. A silicon photodiode monitors the beam intensity that passes through the discharge to record the absorption profile as the laser is tuned. The absorption-line shape is recorded simultaneously with the LIF profile from the thruster plume to provide an unshifted, zero-velocity reference.

Phase-sensitive detection is used to discriminate between the fluorescence and the background emission. A lock-in amplifier is locked to the frequency of a mechanical chopper operating at 2–3 kHz. The highly ionized nature of the plasma results in a low signal-to-background ratio requiring the use of a long time constant ($\tau = 1$ or 3 s) and scan times from 15 to 30 min for the 12-GHz scans. Phase-sensitive detection is also used for the spectrum-tube absorption.

The laser frequency is monitored by a fiber ring interferometer [22] with a 178.4 ± 0.4 MHz free spectral range. A laser-fiber coupler focuses the second beam-splitter reflection into a single-mode fiber connected to the interferometer. Another laser-fiber coupler focuses the interferometer output onto a detector.

3.2 Xenon-ion measurements

Since the 605-nm transition is inaccessible with readily available diode lasers, a tunable dye laser pumped by an argon-ion laser is used for the ion measurements. The dye laser provides linewidths on the order of MHz. As with the above measurements, 1000-mm and 750-mm focal-length lenses focus the 605-nm laser light to a probe volume at the annulus exit of the thruster opposite the cathode. Calculations show the beam waist to be about 50 μm. The approximately 100 mW of laser power that reaches the probe volume again saturates the transition.

The laser beam enters the thruster's annular channel axially and reflects off the anode propellant ring within the thruster. The anode propellant ring is carefully positioned so that the laser beam reflects back on itself through the probe volume. The incoming and reflected beams are then counter-propagating through the probe volume. The resultant fluorescence from the probe volume has two peaks shifted in opposite directions by the Doppler shift. The two profiles are centered around the line center of stationary absorbers. In this situation, a measure of the unshifted line center at the probe volume conditions is provided automatically, and there is no need for an external zero-velocity reference. The reflection is not fully specular. However, as the transition is strongly saturated, the LIF from the reflected beam is comparable to that from the incoming beam.

The same apparatus used for the neutral measurements collects the fluorescence at 529 nm from the probe volume at right angles to the counter-propagating beams. Light is collected over a 1-mm length of the incident and reflected laser beams. The beam diameter determines the other dimensions of the probe volume. The mechanical chopper modulates the probe-beam intensity at 3 kHz, and the lock-in amplifier uses a 3-s time constant. Scan times are 10 min for the 30-GHz scans. The laser frequency is determined by the scan rate of the dye laser's intracavity etalon, with the scan end points obtained by a wavemeter.

4 Results

4.1 Neutral velocities

Figure 6 shows sample simultaneous LIF and absorption traces for the neutral-xenon 823-nm transition. Both measured line shapes have been normalized by the laser intensity and then by their peak values. The LIF is from a probe volume at the center of the Hall-thruster annulus opposite the cathode, 1.5 cm downstream of the exit plane. The absorption is from the xenon spectrum tube serving as the zero-velocity reference. From (1), the line shift of $0.015\ \mathrm{cm}^{-1}$ in Fig. 6 corresponds to a neutral-xenon velocity of $380\ \mathrm{m\,s}^{-1}$ into the laser beam. For a sample condition, the diode laser was tuned up to $0.5\ \mathrm{cm}^{-1}$ from the unshifted or zero-velocity frequency to investigate the possibility of the existence of other collections of neutrals at higher velocities. No signal above the noise level of a few percent of the peak LIF was found.

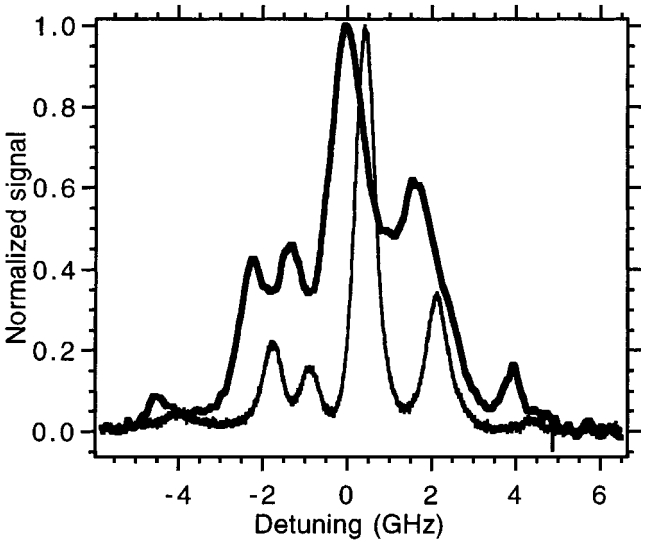

Fig. 6. Frequency shift of neutral-xenon 823-nm-line shape: ▌, LIF from Hall-thruster plume, 1.5 cm from exit plane; ▌, absorption from dc-discharge unshifted-reference source

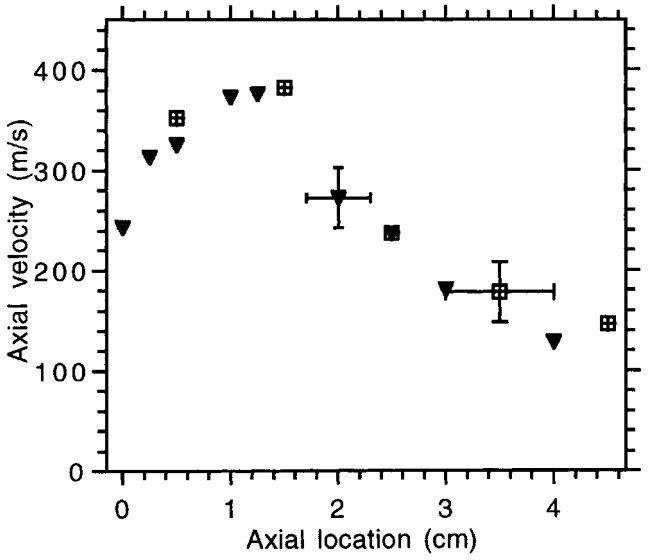

Fig. 7. Neutral-xenon axial velocity at different axial locations: ▼, 6 mm axial probe length; ■, 10 mm axial probe length

Axial neutral velocity calculations from measured line shifts, such as those in Fig. 6, were made at several axial and radial locations under standard thruster operating conditions (see Table 1). The results for the different axial locations, all at the center of the annular channel, are shown in Fig. 7. The exit plane is the position where half of the probe volume is blocked from the collection optics by the edge of the thruster. The location of the probe volume relative to the thruster was measured to within a 1-mm accuracy. The axial velocity was 240 m s^{-1} at the exit plane and peaked near 400 m s^{-1} at 1.0 to 1.5 cm downstream. Two sets of data are shown in Fig. 7, one where the probe volume was 10 mm in the axial direction and one where it was 6 mm. This length is displayed on one point for each data set. The axial velocity measurements for different radial positions were from an axial position 5 mm downstream of the exit plane. These data were all taken with a 6-mm probe length along the laser-beam axis, and the probed locations spanned a 9-mm radial range across the annular channel. The resultant axial velocities were nearly constant, being within 8% of the average value of 330 m s^{-1}.

The Hall thruster was run at different powers to investigate the velocity as a function of discharge current at a point at the center of the annulus 5 mm downstream of the exit plane. The results are shown in Fig. 8. With no solenoid current, a glow discharge could be maintained with 46 mA between the anode and the hollow cathode. As the plasma in a glow discharge is very weakly ionized, the neutral-xenon flow characteristics for this condition are effectively the same as for simple propellant flow with no discharge. The glow discharge is needed, however, to produce the excited-state neutrals required for the LIF measurement. An axial velocity of 100 m s^{-1} was measured in the glow discharge. The thruster body temperature, which was monitored by thermocouples, remained at room temperature throughout this measurement. A measurement was also taken with the thruster running at a power above that of the standard conditions, on the upper part of the V–I curve at 4.7 A and 122 V (see Fig. 4). This elevated power produced a neutral-velocity result significantly higher, reaching 500 m s^{-1}. This operating condition was close to an unstable operating regime.

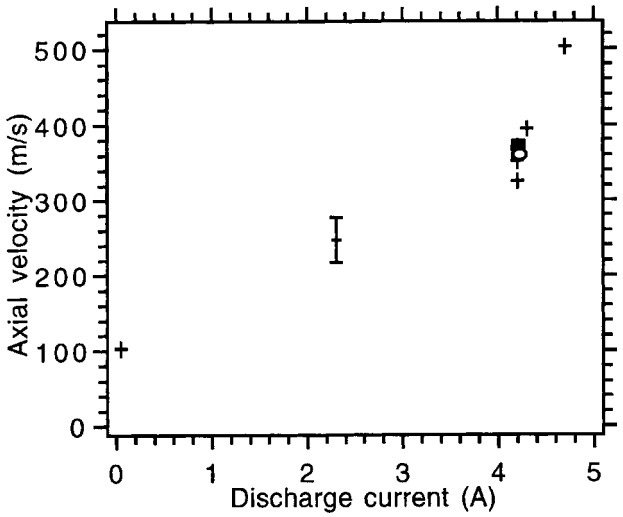

Fig. 8. Neutral-xenon axial velocity 5 mm from exit plane at different operating conditions: +, 2.0 A solenoid current; ○, 1.5 A solenoid current; ■, 1.0 A solenoid current

Included in Fig. 8 are the axial neutral-velocity results for solenoid currents different from the standard conditions. Measurements were made with solenoid currents of 1.0 and 1.5 A as well as with the standard 2.0 A. These solenoid currents correspond to peak magnetic field strengths of 88, 93, and 97 G. The lower magnetic field strengths resulted in line shifts not significantly different from that from the nominal 2.0-A condition. Furthermore, the recorded LIF line shapes for these three different conditions were indistinguishable, within experimental uncertainty.

The main contributing factor to the uncertainty in the axial neutral velocities arises from the determination of the peak position of the recorded LIF data. Noise in the data can cause the maximum measured signal to be slightly offset from where it would have been in a perfectly smooth trace. The frequency locations of the measured LIF traces are found by

matching the overall line shape to a calculated line shape, instead of simply using the peak location. The uncertainty in the placement of the peak location was $\pm 30\,\mathrm{m\,s^{-1}}$. The axial velocity results at different radial positions were consistent with this uncertainty, being constant with a scatter of about this magnitude. The uncertainty is displayed on a sample point for each data set in Figs. 7 and 8. Other contributions to the uncertainty included changes in thruster operation over the scan time, as well as between scans, and the magnitude of the Stark shift. The collisional Stark shift has a linear dependence on the electron number density n_e at the probe volume [23]. An estimate of the Stark shift for the neutral-xenon 823-nm transition can be taken from the line shift versus pressure data of Schwabedissen and Bötticher [24]. If the line shift at the zero-pressure intercept in their data is attributed entirely to a Stark effect, an estimate of the Stark shift can be made. An upper bound of $0.01\,\mathrm{cm^{-1}}$ is obtained at an n_e of $0.8 \times 10^{15}\,\mathrm{cm^{-3}}$. For the smaller n_e values expected at most probed locations in the Hall thruster, the Stark shift arising from interactions with charged particles is anticipated to be small.

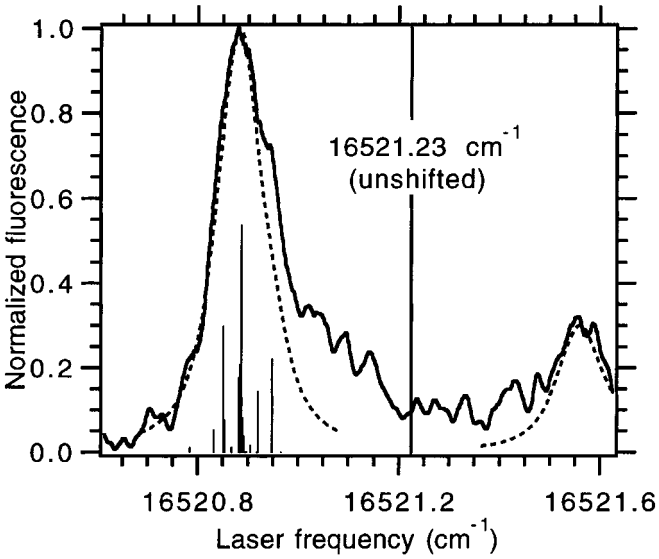

Fig. 9. Frequency shift of xenon-ion 605-nm-line shape: —, LIF from Hall-thruster plume; - - - , constructed profiles; |, lines contributing to the line shape

4.2 Ion velocities

Figure 9 shows a sample trace of the xenon-ion 529-nm fluorescence collected as the laser was tuned over the 605-nm transition. The data has been normalized by the laser intensity and then by the peak value. The LIF is from a probe volume at the center of the thruster channel opposite the cathode, 1.5 cm downstream of the exit plane. The incoming laser beam gave rise to the main fluorescence peak, while the reflection of the beam from the anode propellant ring caused the fluorescence peak at the right side of Fig. 9. The counter-propagating beams produced LIF Doppler shifted in opposite directions. For convenience, profiles for the low laser-power limit were used to establish the peak positions. These constructed profiles are shown with each LIF peak. The hyperfine and isotopic lines contributing to the LIF are shown within one of these profiles. From (1), the line shift in Fig. 9 of $0.34\,\mathrm{cm^{-1}}$ (0.68 cm/2) corresponds to a xenon-ion velocity of $6.2\,\mathrm{km\,s^{-1}}$ in the axial direction. For higher velocities, the two LIF peaks could not be captured in one trace. In this case, two consecutive traces, each recording one of the peaks, were linked using the wavemeter reading. At some of the axial positions far downstream of the exit plane, the reflected beam had diverged to the point where a peak could not be detected clearly. In this case, the peak position of LIF from the incoming beam was compared to the unshifted line center, using an average of all the measurements, to calculate a velocity.

Ion axial velocity data were taken at several axial and radial locations. The thruster was operated near the conditions shown in Table 1. As a consequence of using a current-controlled power supply, however, the discharge voltage varied significantly. Figure 10 shows the results for the different axial locations, all at the center of the annular channel. These velocities correspond to the shifts of the main peaks of LIF. Three sets of data are shown. The first set of data was taken with the main discharge driven by a current-controlled power supply. As indicated on the figure, the discharge voltage drifted from 85 V at the beginning to 78 V for the last measurement. The ion velocity was near $1\,\mathrm{km\,s^{-1}}$ at the exit plane, increasing to near $7\,\mathrm{km\,s^{-1}}$ at 3.0 cm downstream

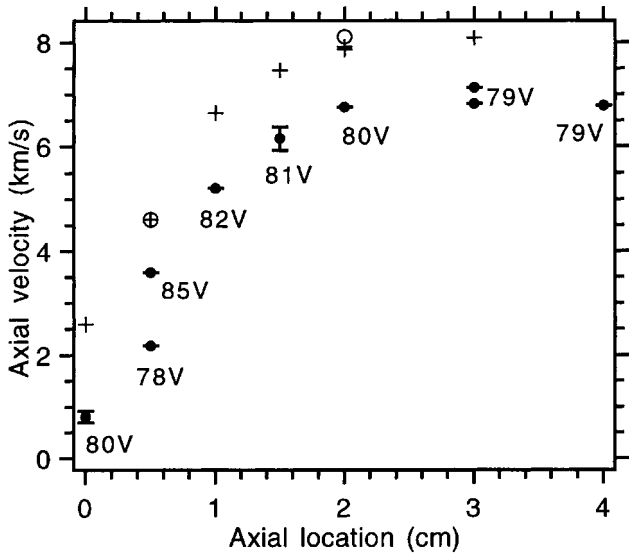

Fig. 10. Xenon-ion axial velocity at different axial locations: •, current-controlled power supply, 4.2 A, voltages as shown; +, voltage-controlled power supply, 88 V, 4.1–4.2 A; ○, current-controlled power supply, 4.2 A, 87 V

before levelling off. The second set of data was taken using a voltage-controlled power supply for comparison. The voltage was set at 88 V in order to match the standard operating current of 4.2 A. This data shows the same trend. The difference in operating voltage resulted from day-to-day changes in the operating conditions of the thruster. Two data points were taken immediately after the second set using the current-controlled power supply at 4.2 A and 87 V for a comparison under more closely matched current-voltage conditions. These conditions gave velocity results similar to the second set, in which the discharge voltage was controlled. Moving radially at a position 0.5 cm from the exit plane, measurements were taken 2, 4, and 5 mm from the center of the annular channel, as well as at the center of the channel. The thruster was operating at 4.2 A and 78 V. The corresponding veloci-

ty results at these different radial positions were within 15% of the 2.2 km s^{-1} value found at the channel center, with no significant trend.

Measurements were also taken at other operating conditions. Using the current-controlled power supply, the thruster was run at higher currents. The results of these measurements are shown in Fig. 11. Measurements were taken at 4.2 and 4.55 A in one session and at 4.2 and 4.73 A in another session. The voltages, which varied from session to session, are shown with each data point. The results at both axial locations show the similar trend of increasing ion velocity with discharge voltage. In another experiment, the thruster was run with decreased xenon-flow rates through the anode, with the voltage-controlled power supply set at a discharge voltage of 155 V. The reduced flow rates allowed for higher discharge voltages and higher resultant ion velocities. Measurements were made at 1.7 mg s^{-1} (2.4 A discharge current), 1.9 mg s^{-1} (2.8 A), 2.1 mg s^{-1} (3.3 A), 2.3 mg s^{-1} (3.7 A), and 2.5 mg s^{-1} (4.4 A) at a position 2.0 cm from the exit plane. The measured velocities were uniform with flow rate, in a range from 11.7 to 12.7 km s^{-1}.

As before, there is an uncertainty in the velocity measurements from the reading of the peak positions of the recorded LIF data. Constructed line shapes are used to help determine where the peak in the data would have been if the trace were perfectly clean. The uncertainty in determining peak locations was ± 100 m s^{-1}. For most measurements, this uncertainty was small relative to the large velocities measured. The wavemeter accuracy also contributes an uncertainty of ± 2 % to each measurement. A sample error bar accounting for these two uncertainties is displayed on two points in Fig. 10 and on one point on Fig. 11. These uncertainties are small compared to changes in ion velocity from changes in thruster operation between different scans. When the thruster operating conditions were carefully matched, the velocity results at a given position were consistent. This result can be seen in Fig. 10 at 0.5 cm and 2.0 cm for the matched conditions. Stark or other shifts of the line center do not contribute to the uncertainty for the ion measurements: The simultaneous recording of LIF from counter-propagating beams automatically calibrates the measurements to account for any non-Doppler line shifts.

4.3 Additional results

The LIF from the counter-propagating beams in the ion velocity measurements provided a measure of the line center, unshifted by the Doppler effect, of the xenon-ion 605-nm transition. This line center corresponds to the point midway between the LIF from the incoming and reflected peaks, as seen in Fig. 9. Twenty-two measurements in total were taken which captured both peaks. There was no discernible trend in the line-center locations with axial position, with radial position, or with discharge operation. The line center from these measurements was found to be 16 521.23 cm^{-1} with a statistical uncertainty (two standard deviations) of 0.01 cm^{-1}. The wavemeter accuracy contributes another 0.01 cm^{-1} to the uncertainty of this value.

The spectral distribution of the measured LIF, or the spectral-line shape, contains information on the velocity distribution of the probed species. To extract information on the kinetic temperature from a Doppler broadening component, an attempt to model the line shape can be made using (4) and the known positions and relative intensities of the isotopic and hyperfine-split lines. For the neutral-xenon-line shapes the kinetic temperature T_{kin} is used as a parameter, along with $\Delta\nu_{\mathrm{L}}$ and a saturation parameter I/I_{sat}. The kinetic temperature determines $\Delta\nu_{\mathrm{G}}$. The saturation parameter mainly affects the relative peak heights in the line shape. The kinetic temperature and $\Delta\nu_{\mathrm{L}}$ affect the width. The saturation parameter needs to be multiplied by factors specific to each of the hyperfine lines through the definition of I_{sat} in (5). These complications, combined with the extensive isotopic and hyperfine splitting, make a full-scale numerical fit intractable; consequently, the parameters are adjusted while comparing the model result to a data trace.

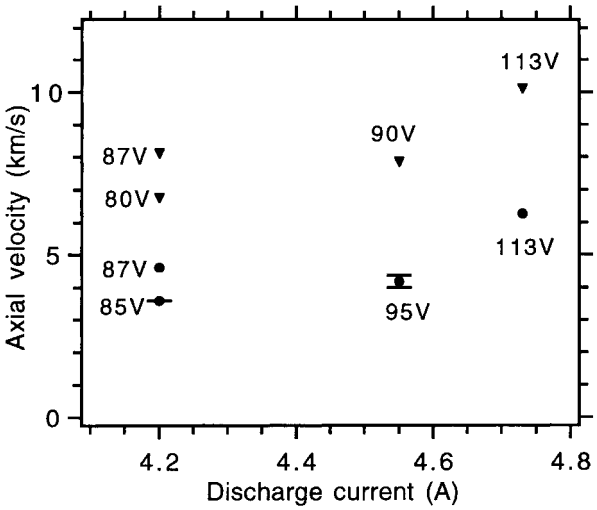

Fig. 11. Xenon-ion axial velocity at different operating conditions: •, 0.5 cm from exit plane; ▼, 2.0 cm from exit plane

A sample neutral-xenon line shape recorded under standard thruster operating conditions was compared to the model. The sample data was taken at the center of the annular channel 1.0 cm downstream of the exit plane. The I/I_{sat} was adjusted to best match the relative peak heights of the three secondary peaks surrounding the main central peak in the 823-nm line shape. Subsequently, $\Delta\nu_{\mathrm{L}}$ and T_{kin} were adjusted to match the width and shape. The model result for an I/I_{sat} of 3.3, a T_{kin} of 500 K, and a $\Delta\nu_{\mathrm{L}}$ of 0.014 cm^{-1} was found to match most closely the experimental spectrum. The results are shown in Fig. 12, in which the data trace from the thruster operating as a glow discharge is also included for comparison. The neutral-xenon kinetic temperature is known to be slightly above room temperature for this low-current glow-discharge condition [4]. Slightly changing $\Delta\nu_{\mathrm{L}}$ from 0.014 cm^{-1} greatly affected the resultant model line shape in comparison to the sample measured spectrum. At T_{kin} values above 700 K, the model-line shape's width became clearly greater than that of the data for a $\Delta\nu_{\mathrm{L}}$ of 0.014 cm^{-1}. The lower temperature boundary is set by the glow-discharge temperature so the neutral-xenon kinetic temperature under standard conditions was 500 ± 200 K.

The neutral-xenon line shapes recorded at standard thruster operating conditions did not show much variation

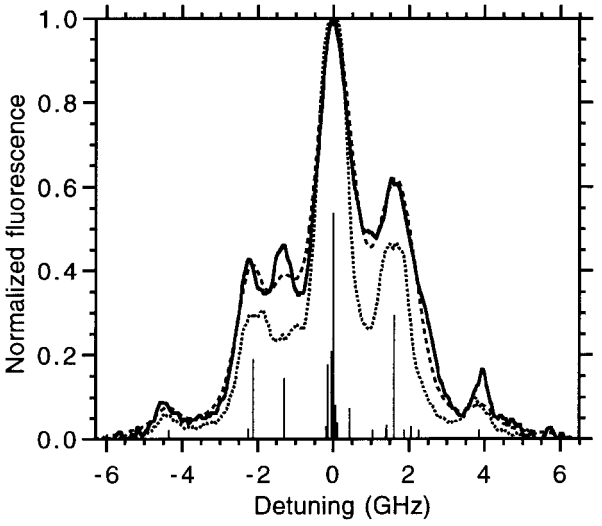

Fig. 12. Neutral-xenon 823-nm saturated-line-shape modelling: —, LIF for standard Hall-thruster operation, 1.0 cm from exit plane; - - -, model result for $T_{\mathrm{kin}} = 500$ K, $I/I_{\mathrm{sat}} = 3.3$, $\Delta\nu_{\mathrm{L}} = 0.014\,\mathrm{cm}^{-1}$; $\cdots$, LIF from Hall thruster operating as a glow discharge

in width. The line shape recorded at a higher thruster power was significantly different, however, having a width corresponding to a temperature that was at least 1000 K. At this condition, 4.7 A and 122 V, the line shape showed no evidence of any underlying structure making it difficult to derive a more definite measure of the neutral kinetic temperature.

From Fig. 9, it is evident that the xenon ions do not have a Maxwellian velocity distribution. No combination of input parameters would construct Voigt profiles to match the recorded LIF data, given the relative locations of the isotopic and hyperfine lines. The non-Maxwellian nature of the distribution is particularly evident on the low-velocity side of the peak LIF signal. Furthermore, constructed profiles that include the effects of saturation cannot possibly replicate this tail in the LIF distribution. The symmetry of the shapes of the LIF peaks about the unshifted line center, accounting for the differences in signal intensities from the incoming and reflected beams, suggests that the non-Voigt shape of each peak arises from a spread in ion velocities rather than from a further splitting of the contributing lines.

A spread of velocities consistently appeared in the recorded xenon-ion data traces. The effect became more apparent for the data taken further from the exit plane, with secondary peaks appearing. The data recorded furthest from the exit plane, 4.0 cm downstream, had a secondary peak of ion LIF comparable to the main peak in signal intensity, at approximately half the peak velocity. The data recorded at different thruster operating conditions were similarly affected, the phenomenon being more a function of location than of power or propellant-flow rate. Substantial secondary peaks were reproduced in data taken consecutively at the same location. Such was the case for the two traces recorded at 2.0 cm from the exit plane with the voltage-controlled power supply, along with the series of traces recorded at 2.0 cm downstream at different flow rates.

5 Discussion

5.1 Velocities

The key information concerning the general operation of Hall thrusters gained from this study is that charge-exchange between accelerated ions and slow-moving neutrals is not substantial. The xenon ions exit the thruster at far higher velocities than the neutrals. The lack of fast-moving neutrals indicates that the ions do not interact significantly with the neutrals exiting the thruster or that low-energy, background neutrals are being entrained into the flow in adequate numbers to thermalize high-velocity neutrals. The insensitivity to thruster operating conditions of the neutral velocities relative to that of the ion velocities is further evidence of the insignificance of the ion-neutral interaction.

Peak ion velocities as high as $12\,\mathrm{km\,s^{-1}}$ are noteworthy for a laboratory-model thruster. The 1.5-kW SPT-100, a thruster nearing space qualification, has ion velocities around $16\,\mathrm{km\,s^{-1}}$ [2]. This thruster was operated at a discharge voltage of 300 V, compared to the 155-V maximum applied to the Hall thruster in this study. For the laboratory-model thruster, the ion acceleration is seen in Fig. 10 to occur mainly over the first 2 cm from the exit plane. This result may be a consequence of the particular design of the magnetic field circuit coupled with the placing of the cathode. These observations demonstrate how these types of measurements can provide insight into thruster operation and aid in an ongoing design process.

The neutrals also accelerate after exiting the Hall thruster, reaching a peak 1.0 to 1.5 cm downstream (Fig. 7). To understand the flow of neutrals, the possibility of momentum-transfer collisions with high-velocity ions and of thermalizing collisions with stationary, background neutrals must be considered. The flow of neutrals is possibly choked at the thruster exit plane. A neutral kinetic temperature of 550 K corresponds to a sonic velocity for xenon of $240\,\mathrm{m\,s^{-1}}$. The neutral velocity may increase after the exit plane from expansion or through collisions with ions. The velocity reduction 1.5 cm downstream might occur because of a shock process or collisions with slower, entrained neutrals. The qualitative observation of the neutral kinetic temperature being axially invariant, however, is evidence against a shock process.

The good agreement between the data sets in Fig. 7 permits two observations. First, the variation in operation of the thruster between the two runs did not noticeably affect the neutral velocities. This result is contrary to that which occurs with the ion velocity, further indicating only a small interaction between the ions and the neutrals. The ion velocities are very sensitive to changes in thruster operation, specifically the discharge voltage. Secondly, there are no steep gradients in the density of excited neutrals. The measured line shift and corresponding velocity are skewed to those in the region of the highest density of absorbers within the probe volume, because that region dominates the fluorescence. High density gradients would cause disagreement in the measured velocity at some axial locations between data taken with probe volumes of different sizes.

The neutral flow is affected by significant changes in the power input to the thruster, but not notably by changes in magnetic field. With xenon flowing through the thruster when it is not operating, the measured velocity of $100\,\mathrm{m\,s^{-1}}$

at 5 mm downstream of the exit plane is subsonic. The xenon sonic velocity in a room-temperature glow discharge is $180\,\mathrm{m\,s^{-1}}$. In contrast, for the standard operating conditions it was shown above that the flow is possibly sonic at the exit plane and increases downstream. When the thruster is pushed to operate at a point further up from the voltage knee, the velocity 5 mm downstream increases significantly. The higher velocity may result from the increase in the velocity of the ions interacting with the neutrals; alternatively, it may be from an increase in the heating of the neutrals, resulting in higher velocities independent of a more direct interaction of neutral velocities with the ions. Changing the magnetic field should affect thruster performance. Therefore, the observed insensitivity of the neutral axial velocities to the applied magnetic field further suggests a lack of interaction of the neutrals with the ions.

As discussed previously, changes in the discharge voltage as a result of the unsteady thruster operation must be considered. The ion velocity results are reproducible for conditions where the voltage is matched. The data in Fig. 10 for 87–88 V at 0.5 and 2.0 cm demonstrate this observation. Differences between the data sets taken with the current- and voltage-controlled power supplies are attributable to differences in discharge voltage. As seen in Fig. 11, increasing the current affects the ion velocity through its relation to the discharge voltage. In contrast, the ion velocity is not sensitive to radial position, nor to the investigated changes of as much as 50% in flow rate. The ion acceleration being external to the channel may serve to make these factors unimportant.

5.2 Velocity distributions

The effect of saturation on the line shapes obtained in this study limits the accuracy of the determination of plasma parameters from line-shape analysis. Many of the assumptions implicit in (4) become disputable for saturated-line shapes and for the conditions of interest. A more refined model for a saturated-line shape would require a better knowledge of the plasma conditions. Changes in thruster operation which may affect the excited-state neutral-xenon populations over the long scan times also contribute to discrepancies between a measured spectrum and a model. Further, a significant assumption in the model is that of a Maxwellian velocity distribution of the neutrals in the probe volume. The assumption of translational equilibrium at a point in the plasma may be questionable in itself, but the assumption that the neutrals throughout the probe volume have an equilibrated velocity distribution is idealistic. The probe volume being larger than the region over which there is a substantial velocity change, or change in Doppler shift, can result in a blended line shape. This complication makes the model's applicability to the line shape recorded at higher thruster powers more questionable as there are larger velocity gradients in the probe volume.

It is, nevertheless, possible to extract some information on the neutral-xenon kinetic temperature. From Fig. 12, it can be seen that the width of the recorded spectrum from Hall thruster operation is slightly greater than that of the spectrum from glow-discharge operation. Thus, the 500 ± 200 K result is reasonable because, as previously discussed, the kinetic temperature in the glow-discharge case is known to be near room temperature. From calculations for the 823-nm transition, Stark broadening of $0.014\,\mathrm{cm^{-1}}$ is predicted to correspond to an electron number density on the order of 10^{14}–$10^{15}\,\mathrm{cm^{-3}}$ [24, 25], which is a possibility for some locations in the Hall discharge. This value for $\Delta\nu_\mathrm{L}$ of the line shape is thus not unreasonable for use in the determination of the kinetic temperature.

An examination of the xenon-ion line shapes leaves no doubt that the ion-velocity distribution is non-Maxwellian. A kinetic temperature cannot be defined. The majority of ions travel at the peak velocity; however, the remainder apparently leave the thruster with a range of velocities mainly below this peak velocity. The xenon ions accelerate across the potential drop in the discharge from the location where they are created. The LIF spectrum reflects, in part, the distribution of the potential drops over which the ions accelerate, and in turn reflects the locations where they are created. The spectrum reveals that the majority of ions are created at one axial location, with some being created downstream from this point. Collisions may slightly affect this distribution. Plasma oscillations in the thruster may also contribute to the distribution of ion velocities. Prior research has found that ions may not exit Hall thrusters at a constant velocity. Plasma oscillations in the tens of kHz modulate the velocity of the ions [26, 27]. As the LIF measurements made here do not have that time resolution, the effect of the oscillations on the measurements would be a spreading of the line shape in the observed velocity space. Charge-exchange of fast-moving ions with slow-moving, background neutrals could be another possible explanation for a spread in ion velocities. The neutral data, however, show ample evidence to discount this possibility.

As discussed, the validity of the assumption of a Maxwellian velocity distribution is an important consideration in the analyses of the neutral- and ionic-xenon line shapes. This assumption comes into question for the axial measurements made here because of distributions in the axial velocity. Probing the plasma circumferentially may circumvent these difficulties. Velocity gradients across the probe volume would be small because of small circumferential velocities. There would be no difference in acceleration from different potential drops that the ions had encountered. The ions would still have a modulated velocity due to plasma oscillations, but probably not on the same scale as in the axial direction. The distribution of velocities in the probe volume would be predominantly determined by thermal considerations, not by gradients, varied potential drops, or plasma oscillation effects. Thus, to better assess the kinetic temperature of either species, measurements should be made with the laser probing the thruster plume circumferentially. However, this arrangement would yield circumferential – not axial – velocity information.

5.3 Additional spectroscopic details

Previously published values for the line center of the probed xenon-ion transition are $16\,521.22\,\mathrm{cm^{-1}}$ [9] and $16\,521.24\,\mathrm{cm^{-1}}$ [8]. The value found in this study is $16521.23(\pm 0.02)\,\mathrm{cm^{-1}}$, in agreement with the values from the literature. This result shows the Stark shift to be negligible for this ion transition under the plasma conditions in the thruster plume, particularly in relation to the magnitude of the observed Doppler shifts. The lack of a trend in the line-center locations further enforces this observation.

As discussed earlier, the Stark shift arising from interactions with charged particles for the neutral-xenon transition is also not expected to be significant. It is possible, though, that a Stark shift has a slight effect on the velocities calculated at some locations. The measured line shift is slightly, but not significantly, higher for the lower applied magnetic fields. The lower solenoid currents may result in lower local electric field, E, and n_e values in the probe volume and thus smaller Stark shifts. If this observation is attributable to an actual occurrence and not just to the uncertainty in the measurement, it would indicate a Stark shift of the main lines of the 823-nm transition in the opposite direction in frequency from that of the Doppler shift. A Stark shift in this direction would offset some of the Doppler shift, resulting in a slight underestimate of the velocity. However, the neutral-xenon line shapes give no evidence of a Stark shift. As seen in Fig. 12, the relative locations of the nuclear-spin-split lines agree with their unshifted relative positions: There is no indication that these components are shifted by different amounts or in opposite directions by the Stark effect. Furthermore, no change is observed in the overall measured line shape due to different relative Stark shifts as the local E and n_e change with the different applied magnetic fields.

The spectral distribution of the fluorescence from the thruster plume contains information on other plasma parameters besides the kinetic temperature, such as the electron number density and magnetic field. The electron number density determines the Lorentzian width of the transitions through Stark broadening; however, the broadening rate and confidence in the model result for $\Delta\nu_L$ are both lacking. The effects of the magnetic field are not readily apparent. The qualitative observation of the replication of the recorded neutral-line shape at different magnetic field strengths indicates that the Zeeman splitting is not significant for the given operating conditions. The Zeeman splitting is also negligible for the ion as it is of similar magnitude to that of the neutral.

Acknowledgements. This work was supported by the United States Air Force Office of Scientific Research, Aerospace Sciences and Materials Directorate. W.A.H. acknowledges funding from the United States Air Force Palace Knight Program.

References

1. P.V. Storm, M.A. Cappelli: Appl. Opt., submitted for publication (Mar. 1997)
2. D. Manzella: AIAA-94-3141, 30th Joint Propulsion Conference, Indianapolis, IN, USA (June 1994)
3. M.S. Rhee, M.J. Lewis: AIAA-95-2928, 31st Joint Propulsion Conference, San Diego, CA, USA (July 1995)
4. R.J. Cedolin, R.K. Hanson, M.A. Cappelli: Phys. Rev. A **54**, 335 (1996)
5. C.R. Bingham, M.L. Gaillard, D.J. Pegg, H.K. Carter, R.L. Mlekodaj, J. Cole, P.M. Griffin: Nucl. Instrum. Methods **202**, 147 (1982)
6. C. Borghs, P. De Bisschop, R.E. Silverans, M. Van Hove, J.M. Van den Cruyce: Z. Phys. A **299**, 11 (1981)
7. S.D. Rosner, T.D. Gaily, R.A. Holt: Phys. Rev. Lett. **40**, 851 (1978)
8. C.E. Moore: *Atomic Energy Levels*, National Bureau of Standards Circular 467 (U.S. GPO, Washington 1958), Vol. III, p.113
9. J.E. Hansen, W. Persson: Physica Scripta **36**, 602 (1987)
10. R.P. Lucht, in *Laser Spectroscopy and its Applications*, edited by L.J. Radziemski et al. (Marcel Dekker, Inc., New York 1987), pp.623–7
11. J.O. Berg, W.L. Shackleford: Appl. Opt. **18**, 2093 (1979)
12. A. Yariv: *Quantum Electronics*, 3rd ed. (Wiley, New York 1989), pp.168–70
13. A.E. Siegman: *Lasers* (University Science Books, Mill Valley, CA 1986), pp.207–295
14. M. Mitchner, C.H. Kruger, Jr.: *Partially Ionized Gases* (Wiley, New York 1973), p.70
15. H.R. Kaufman: AIAA Journal **23**, 78 (1985)
16. H.R. Kaufman, R.S. Robinson, M.L. Day, T.W. Haag: AIAA-90-2595, 21st International Electric Propulsion Conference, Orlando, FL, USA (July, 1990)
17. J. Ashkenazy, Y. Raitses, C. Appelbaum: AIAA-95-2673, 31st Joint Propulsion Conference, San Diego, CA, USA (July 1995)
18. J.J. Szabo, J.E. Pollard: AIAA-95-2926, 31st Joint Propulsion Conference, San Diego, CA, USA (July 1995)
19. A. Bober, N. Maslennikov: IEPC-93-00l, 23rd International Electric Propulsion Conference, Seatlle, WA, USA (Sept. 1993)
20. E.A. Pinsley, C.O. Brown, C.M. Banas: J. Spacecraft **1**, 525 (1964)
21. J.C. Camparo: Contemp. Phys. **26**, 443 (1985)
22. L.F. Stokes, M. Chodorow, H.J. Shaw: Opt. Lett. **7**, 288 (1982)
23. H.R. Griem: *Spectral Line Broadening by Plasmas* (Academic Press, New York 1974), p.320
24. A. Schwabedissen, W. Bötticher: J. Phys. B **26**, 3467 (1993)
25. J. Purić, S. Djeniže, J. Labat, A. Srećković, M. Platiša: Contrib. Plasma Phys. **31**, 63 (1991)
26. G.S. Janes, R.S. Lowder: Phys. Fluids **9**, 1115 (1966)
27. Y.B. Esipchuk, A.I. Morozov, G.N. Tilinin, A.V. Trofimov: Zh. Tekh. Fiz. **43**, 1466 (1973) [Sov. Phys. Tech. Phys. **18**, 928 (1974)]